Crystalline Structure of Injection Molded β-Isotactic Polypropylene Analysis of the Oriented Shear Zone

DATASET · OCTOBER 2014

READS
74

7 AUTHORS, INCLUDING:

Xianhu Liu
Friedrich-Alexander-University of Erlangen-Nü…
14 PUBLICATIONS **75** CITATIONS
SEE PROFILE

Kun Dai
Zhengzhou University
62 PUBLICATIONS **432** CITATIONS
SEE PROFILE

Guoqiang Zheng
Zhengzhou University
68 PUBLICATIONS **273** CITATIONS
SEE PROFILE

Changyu Shen
Indiana University School of Medicine
166 PUBLICATIONS **2,686** CITATIONS
SEE PROFILE

I&EC research
Industrial & Engineering Chemistry Research

Article

pubs.acs.org/IECR

Crystalline Structure of Injection Molded β-Isotactic Polypropylene: Analysis of the Oriented Shear Zone

Xianhu Liu,[†,‡,§] Kun Dai,[†] Xiaoqiong Hao,[‡] Guoqiang Zheng,*[,†] Chuntai Liu,*[,†] Dirk W. Schubert,[‡] and Changyu Shen[†]

[†]College of Materials Science and Engineering, The Key Laboratory of Material Processing and Mold of Ministry of Education, Zhengzhou University, Zhengzhou, 450002, P.R. China

[‡]Institute of Polymer Materials, Friedrich-Alexander University Erlangen-Nuremberg, Martensstrasse 7, 91058 Erlangen, Germany

Supporting Information

ABSTRACT: Although both shear flow and β-nucleating agent (β-NA) could separately induce β-crystal in isotactic polypropylene (iPP), their combination, particularly in the typical industrial processes, in fact has received comparatively little attention. In the current study, two-dimensional wide-angle X-ray diffraction and small-angle X-ray scattering (2D-WAXD/SAXS) measurements were performed to investigate the effect of β-NA on the crystalline structure of the oriented shear zone in injection molded iPP. It is observed that, regardless of the β-NA concentration, parent−daughter structure of α-crystal can be formed in iPP. Furthermore, the fraction of daughter lamellae elevates with the increasing concentration of β-NA. Interestingly, unexpected scattering patterns of (300) reflection for β-crystal, which is similar with that for parent−daughter lamellar branching of α-crystal, is exclusively found in iPP with higher concentration of β-NA (1.0 wt %). The most possible explanation is that the addition of high content of β-NA lowers the free energy barrier. Additionally, the same change tendency of long period, crystal lamellar thickness and lateral dimension, *d*-spacing and crystallite size is found, viz., they first increase and then decrease with the increasing β-NA content. The results demonstrate that the concentrations of β-NA have a significant effect on the crystal grain structure under the practical molding process.

INTRODUCTION

Isotactic polypropylene (iPP) is well-known a very important commercial polymer with low manufacturing cost and rather versatile properties. So far, it has been demonstrated that there are at least four typical crystalline modifications, namely, α, β, γ, and smectic mesophase,[1−3] for iPP. Among these crystalline modifications, β-form might be the most fascinating one due to its excellent toughness and ductility. Thereby, many researchers are interested in this topic.[4−13] Compared with the α-crystal obtained under common processing conditions, a higher level of β-crystal can be only generated under some special conditions, such as shear-induced crystallization,[4−6] temperature gradient,[7] and the addition of β-nucleating agent (β-NA).[8−13] Generally speaking, the addition of β-NA is the most effective and accessible method to obtain a higher content of β-crystal in iPP.

Processing methods strongly affect the final microstructure of semicrystalline polymers (e.g., iPP, HDPE, and so on). In most processing operations, a molten polymer is subjected to an intense flow field and will crystallize during or after being imposed to flow. As an example, injection molding is the most common and convenient processing operation to manufacture polymer articles with regular geometric profiles. It is well-known that there exists a "skin-core" structure in the molded samples, especially for iPP, because of the shear and thermal gradients.[14−17] The amorphous "skin" is very thin due to a rapid cooling rate, while a lower cooling rate and a more feeble flow in the "core" allow complete relaxation of chains and consequent growth of spherulites. Between the thin "skin" and broad "core", a shear zone forms which usually comprises a highly oriented structure. In particular, providing favorable conditions are involved, a branched shish-kebab structure can also be developed in the shear zone of the injection molding part.[16]

The macroscopically hierarchical structure of an injection molded sample has been intensively investigated over the past two decades because such multiple layers are crucial for the end-use properties of the molded articles. Unfortunately, although shear flow plays a very important role in the formation of a β-crystal, only a small amount of β-crystal can be formed in the shear zone of the injection molded parts due to the larger cooling rate.[17]

Flow-induced crystallization in iPP has been extensively studied under precisely controlled conditions (e.g., Linkam CSS 450 shear cell).[18−20] However, under the typical industrial processes, flow-induced crystallization becomes more complicated, particularly in the presence of β-NA. The presence of β-NA has significant influences on this process and eventually affects the final microstructure of the resultant articles. To the best of the authors' knowledge, the role of β-NA under flow field on the crystalline structure, especially in the oriented shear zone, has received little attention. Thus, in this study, we are interested in the role of the concentration of β-NA in the formation of crystalline structure under the complex thermo-mechanical conditions in the oriented shear zone of injection

Received: April 12, 2013
Revised: July 22, 2013
Accepted: August 4, 2013
Published: August 5, 2013

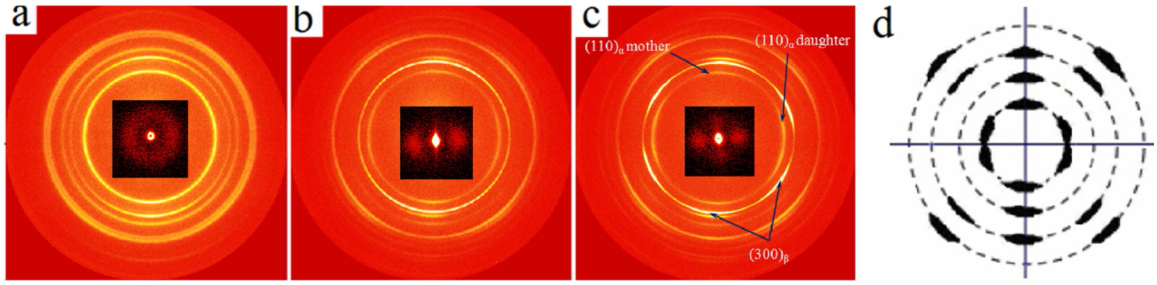

Figure 1. 2D-WAXD patterns of (a) iPP-0.0, (b) iPP-0.2, and (c) iPP-1.0 and (d) the schematic of 2D-WAXD patterns of oriented parent−daughter structure in α-iPP according to ref 16. The insets show the corresponding 2D-SAXS pattern.

molded iPP. The understanding of this process is of practical significance, especially for the cases where severe stress and extreme change of temperature field are simultaneously involved.

EXPERIMENTAL METHODOLOGY

Materials. A commercially available iPP (T30S) was bought from Lanzhou Petrochemical, which has a melt flow index of 2.6 g/10 min (190 °C, 21.6 N) and $\overline{M}_n$ = 11.0 × 10^4 g/mol. The β-NA, a kind of rare earth organic complex (WBG), was kindly provided by Guangdong Winner Functional Materials, China. It is a kind of irregular block-like crystal. Most of the agglomerates consist of several fibril-like crystals and its single crystal diameter is about tens of nanometers (see Figure S1 in Supporting Information).

Sample Preparation. The iPP was melt mixed with 0.2 and 1.0 wt % β-NA by a twin-screw extruder (Giant, SHJ-20B, the L/D ratio = 20 and D = 20 mm). The screw speed was 110 rpm, and the temperature profile from hopper to die was 150, 160, 170, 185, 195, and 190 °C, respectively. A HTF80B−W2 injection molding machine (Haitian, China) was used for melt injection. The barrel temperature was 170, 185, 205, and 200 °C, respectively, from the hopper to nozzle.

According to the coordinate directions in polymer flow, there are three flow models: one-dimensional flow, two-dimensional flow, and three-dimensional flow. Among them, one-dimensional flow is the simplest one, such as the polymer flow in the tubular channel cavity (well-known as channel Poiseuille flow). The main objective of this study is to investigate the crystalline morphology of β-iPP under shear field in practical processing. For this purpose, a mold with tubular channel cavity was intentionally designed and used in this study. The samples' profile is of cylindrical shape, with a diameter of 10 mm and a length of 300 mm. The injection molded samples were labeled as iPP-0, iPP-0.2, and iPP-1.0, corresponding to the β-NA concentrations of 0%, 0.2%, and 1.0% by weight, respectively.

Characterization. Two-dimensional wide-angle X-ray diffraction (2D-WAXD) measurements were carried out using U7B beamline at room temperature in the National Synchrotron Radiation Laboratory (NSRL) of the University of Science and Technology of China (USTC). The chosen X-ray wavelength was 0.154 nm. A MAR 345 image plate detector was employed to collect all the 2D-WAXD images. Two-dimensional small-angle X-ray scattering (2D-SAXS) measurements were carried out using a NanoSTAR-U (Bruker AXS Inc.) with Cu Kα radiation source (λ = 0.154 nm) at room temperature. Its generator was operated at 45 kV and 650 μA.

Before 2D-WAXD and 2D-SAXS measurements, a segment with 10 mm length (i.e., the flow direction, FD) is cut in the middle of the part, from which a board of 1 mm thickness was ground along FD-RD (wall direction) plane. The schematic of sample preparation for measurements can be found in Figure S2 in the Supporting Information of this study and ref 21. The selected position for measurement was taken at 100 μm away from the skin surface along the RD, named as shear zone, due to the following reasons: (1) it has been found that a branched shish-kebab structure is formed in this position for pure iPP in our previous paper;[21] (2) it has been well proven that the shish-kebab structure emerges roughly 100 μm from the surface of samples, regardless of the thickness of samples.[22] The X-ray beam is perpendicular to the FD-RD plane. It should be noted that 2D-WAXD and SAXS tests were performed in the same position.

The orientation parameter was calculated using the Herman's orientation parameter, which is defined as follows:[23]

$$f = \frac{(3\langle\cos^2\phi\rangle - 1)}{2} \tag{1}$$

where $\langle\cos^2\phi\rangle$ is an orientation factor defined as

$$\langle\cos^2\phi\rangle = \frac{\int_0^{\pi/2} I(\phi)\cos^2\phi\sin\phi\,\mathrm{d}\phi}{\int_0^{\pi/2} I(\phi)\sin\phi\,\mathrm{d}\phi} \tag{2}$$

where $I(\phi)$ is the scattering intensity at ϕ. The orientation parameters are calculated by eqs 1 and 2 from the scattering intensity distribution along the azimuthal angle between 0° and 360°.

To get more insights into crystallization, the peak-fit procedure was used to deconvolute the peaks in the 1D-WAXD profile. Herein, the X-ray curves were resolved into crystalline and amorphous peaks. The overall crystallinity, X_c, was calculated by

$$X_c = \frac{\sum A_{\mathrm{cryst}}}{\sum A_{\mathrm{cryst}} + \sum A_{\mathrm{amorp}}} \tag{3}$$

where A_{cryst} and A_{amorp} are the fitted areas of the crystalline and amorphous phases. The relative content of β-crystal, K_β, can be quantitatively evaluated by Turner-Jones criterion defined as follows:[24]

$$K_\beta = \frac{A_{\beta(300)}}{A_{\alpha(110)} + A_{\alpha(040)} + A_{\alpha(130)} + A_{\beta(300)}} \tag{4}$$

where $A_{\chi(hkl)}$ represents the area of the (hkl) peak belonging to the α- or β-crystal. Meanwhile, the crystallinity of β-crystal (X_β) and the crystallinity of α-crystal (X_α) are given by

$$X_\beta = K_\beta X_c \tag{5}$$

$$X_\alpha = X_c - X_\beta \quad (6)$$

RESULTS AND DISCUSSION

Orientation. Figure 1a–c shows 2D-WAXD patterns obtained from shear zone of iPP-0.0, iPP-0.2, and iPP-1.0. It can be clearly seen that, in contrast to pure sample (iPP-0), apparent arc-like diffractions are seen in the β-iPP samples (iPP-0.2 and iPP-1.0), indicative of obvious molecular orientation. For example, the azimuthal widths in the intensity of (040) reflections are relatively narrow in β-iPP samples (see Figure 2), which is indicative of higher molecular orientation in the α-crystal. This can be further confirmed by the calculated orientation parameters shown in Table 1.

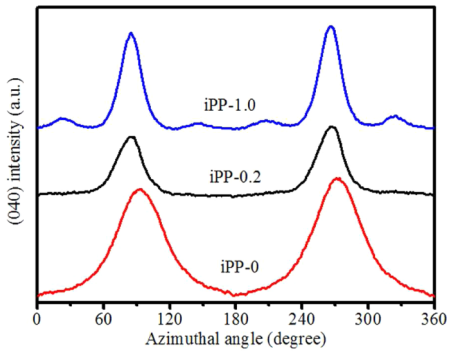

Figure 2. Traces showing the variation in intensity of the (040) reflections as a function of the azimuthal angle.

Table 1. Orientation Parameter, Fraction of Daughter Lamellae (R) and Parent–daughter Ratio ($[R]$) for Different β-NA Contents in iPP Samples. Definitions of R and $[R]$ Are Given in eqs 7 and 8

samples	f_{WAXS}	f_{SAXS}	R	$[R]$
iPP-0	0.51	0.32	0.68	0.48
iPP-0.2	0.82	0.72	0.65	0.52
iPP-1.0	0.89	0.85	0.48	1.06

To analyze the crystalline lamellar orientation, 2D-SAXS measurements were conducted, and the corresponding 2D-SAXS patterns are shown in the inset of Figure 1 panels a–c. For β-iPP samples, two distinct maxima along equatorial and meridional directions are observed. It is generally accepted that the merdional streak is attributed to the formation of the shish parallel to the flow direction and the equatorial maximum is ascribed to the kebab structure perpendicular to the flow direction.[25,26] Thus, Figure 1 reveals the formation of the obvious shish-kebab structure and higher lamellar orientation (see Table 1) in the β-iPP samples.

It is well-known that oriented structure cannot be formed without the action of flow, and likewise it cannot be induced by direct addition of nucleating agent. Whereas, during flow, the nucleating particles will influence the distribution of local stress which can substantially enhance the molecular orientation in the vicinity of nucleating particles.[17,27] The reason is as follow: in our case, β-NA presents the solid state at 200 °C,[28] therefore, the local shear can be caused by different velocities at the interface between molten iPP and solid β-NA. Accordingly, compared to iPP-0.0 melt, the local shear is responsible for the enhancement orientation of iPP-0.2 and iPP-1.0. On the other hand, the nucleating agent could lower the free energy barrier for the formation of shish or secondary nucleation.[29,30] Accordingly, owing to the aforementioned reasons, the fact that the addition of β-NA leads to such well-pronounced crystal orientation is understandable.

Parent–Daughter Structure. Lamellar branching has been observed over a wide range of crystallization conditions,[16,19,25,26,31–34] which has always been considered as a general characteristic of α-iPP crystallization. Many studies have shown that lamella-branched shish-kebabs can be formed in the shear zone of injection molded samples.[25,26,32,33] In our previous work,[21] such lamellar branching was also found in the shear zone of a pure iPP sample. Unfortunately, the underlying mechanism was not further discussed. Herein, the azimuthal scans of (110) integrated from the 2D-WAXD patterns shown in Figure 1 are present in Figure 3. Clearly, the

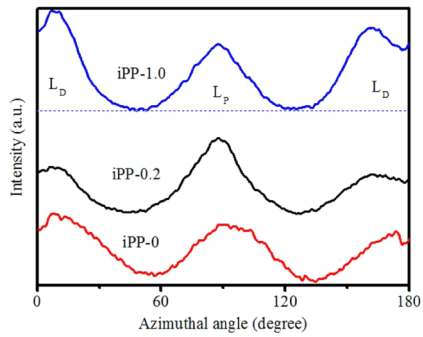

Figure 3. Traces showing the variation in intensity of the (110) reflections as a function of the azimuthal angle.

(110) intensity curve shows bimodal maxima at 0° and 180° and another maxima at 90°, which is indicative of a mixed bimodal orientation for α-crystals. As illustrated in the classical schematic of a 2D-WAXD of an oriented parent–daughter structure in α-iPP (see Figure 1d), such mixed bimodal orientation is regarded as a parent–daughter model according to the bimodal (110) reflections. That is, parent lamellae is preferentially oriented in the flow direction, and the daughter lamellae is preferentially perpendicular to the flow direction.[16,25,26,31,33,34] In short, the observed scattering is strictly consistent with the proposed structural model presented in Figure 1d. Therefore, the above results confirm that the lamella-branched shish-kebab structure exists in a α-crystal for all samples, being independent of the β-NA concentrations.

A comparison between parent lamellae and daughter lamellae orientation will be done via an evaluation of the fraction of daughter lamellae (R) which can be evaluated from the azimuthal scan curve of the (110) reflections according to the following method:[16]

$$R = \frac{A^*}{C + A^*} \quad (7)$$

where A^* is taken as the area around an azimuthal angle of 0° and C represents the area around 90° after subtraction of the baseline area (see Figure 3). Meanwhile, according to the method proposed in reference 32, the ratio of parent lamellae and daughter lamellae ($[R]$) is estimated as follows:

$$[R] = \frac{C}{A^*} \quad (8)$$

As listed in Table 1, it is clear that R decreases with the introduction of β-NA while the behavior of $[R]$ is opposite.

dx.doi.org/10.1021/ie401162c | Ind. Eng. Chem. Res. 2013, 52, 11996–12002

This phenomenon is more remarkable at higher concentrations of β-NA, suggesting that daughter lamellae in α-crystals are prevented by the introduction of β-NA. As mentioned above, the presence of β-NA provides the lower free energy barrier at which lower level shear flow would be sufficient to induce more shish in the melt, and subsequently generates an epitaxial growth of folded chain lamellae. Besides, $[R]$ is strongly influenced by shear flow.[19] On the other hand, the kebab will grow after the cessation of flow. Thus, it is conceivable that more β-NA content prevents more daughter lamellae of the α-crystal epitaxially grown on the parent lamellae.

Figure 4 shows the azimuthal profiles of the (300) reflection. Together with Figure 1, Figure 4 shows that there are two

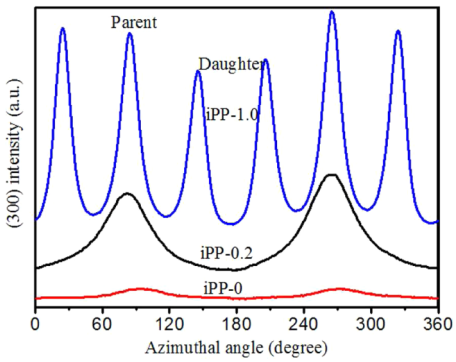

Figure 4. Traces showing the variation in intensity of the (300) reflections as a function of the azimuthal angle.

obvious diffraction arcs and peaks in iPP-0.2, while there are six arcs and peaks in iPP-1.0, which indicates a different crystalline morphology of β-crystal for the two samples. The two-peak azimuthal profile in iPP-0.2 indicates molecular orientation of the β-crystal along the flow direction, while the six-peak azimuthal profile in iPP-1.0 suggests at least two kinds of molecular orientation for the β-crystal. Clearly, analogous to the definition of a parent−daughter model of the α-crystal, the reflection peaks at ca. 30° and 150° may originate from the "daughter lamellae" of the β-crystal, and the reflection peak at ca. 90° may originate from the "parent lamellae". The fraction of daughter lamellae and the parent−daughter ratio are 1.33 and 0.75, respectively. Herein, iPP-1.0 has the lowest parent−daughter ratio (0.75), suggesting the existence of fewer β-crystal "parent lamellae" and less space for nucleation,[32] but more space for "daughter lamellae" of the β-crystal to grow. Considering that increasing the content of β-NA will lower the free energy barrier, the fact that the growth of "daughter lamellae" in the β-crystal confines the growth of "parent lamellae" can therefore explain this.[34] On the other hand, the presence of nucleating agent may amplify the local shear intensity at the interface.[35] However, to the best of the authors' knowledge, the appearance of a six-arcs pattern of β-crystal is scarcely elucidated in depth in the open literature, and further study on the underlying origin for this is undergoing in our group.

Crystallinity. It is believed that β-NA-induced rich nucleation for high β-crystal content due to strong heterogeneous nucleation,[12,13] and the nucleation rate of iPP could be also effectively enhanced by the flow field. From the analysis of the diffraction peak positions and integrated peak intensities, the crystals composition in the shear zone is determined. As shown in Figure 5, for iPP-0, only peaks of α-crystal are

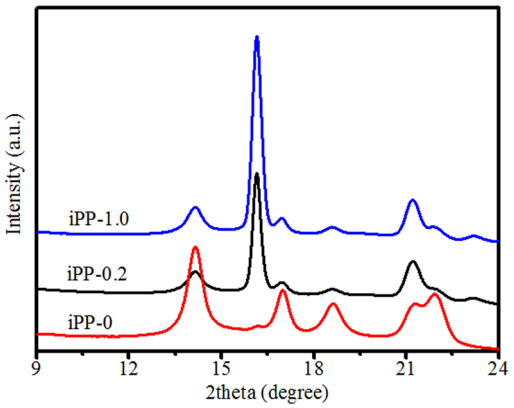

Figure 5. Corresponding 1D-WAXD curves obtained from 2D-WAXD patterns.

observed, whereas those of α- and β-crystal coexist in the β-iPP samples. X_β in iPP-0 is negligibly small. But, in iPP-0.2 and iPP-1.0, higher X_β of 0.43 and 0.53 are found. Meanwhile, one observes a moderate increase in X_c with a continuous increase of the β-NA concentrations from 0 to 1.0 wt % (see Table 2).

Table 2. The Overall Crystallinity, Crystallinity of α-Crystal and β-Crystal for Different β-NA Contents in iPP Samples

sample	X_c	X_α	X_β
iPP-0	0.60	0.59	0.01
iPP-0.2	0.64	0.21	0.43
iPP-1.0	0.70	0.17	0.53

Accordingly, it demonstrates that the addition of β-NA not only induces the generation of β-crystal serving as the β-nucleating agent, but also increases the overall crystallinity. A similar trend has been reported by some of the literature.[35−38]

Long Period. Lorentz-corrected intensity profiles of circularly integrated 2D-SAXS patterns of iPP-0, iPP-0.2, and iPP-1.0 are shown in Figure 6. Unexpected results can be found

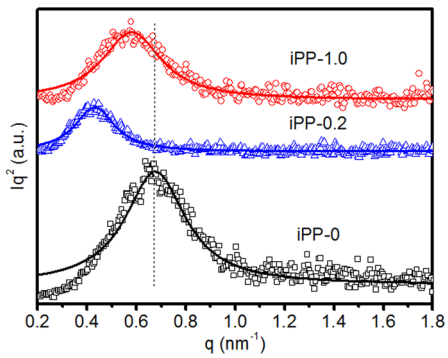

Figure 6. Lorentz-corrected 1D-SAXS intensity profiles. Solid lines are fitted data using the Lorentz method.

that, with the increase of β-NA content, the position of the scattering peak shifts to a lower q value (q is the scattering vector) in iPP-0.2, while it shifts to the original position in iPP-1.0. The long period (L) is related with the position of the scattering peak, which can be calculated using the Bragg's law:

$$L = \frac{2\pi}{q_{max}} \quad (9)$$

dx.doi.org/10.1021/ie401162c | Ind. Eng. Chem. Res. 2013, 52, 11996−12002

The crystal lamellar thickness, l_c, is also determined according to the method:[15]

$$l_c = X_c L \tag{10}$$

Because the crystallinity of all samples in this study is higher than 50% (see Table 2),[39,40] l_a is therefore assigned as the smaller value and l_c can be obtained by $l_c = L - l_a$. The calculated results are shown in Table 3.

Table 3. Long period, Average Thickness of the Amorphous and Crystalline Lamellae, and Lateral Dimension of Crystalline Lamellae for Different β-NA Contents in iPP Samples

sample	L_{bragg}(nm)	l_a (nm)	l_c (nm)	D (nm)
iPP-0	9.3	5.7	4.2	16.4
iPP-0.2	14.4	9.4	5.0	28.6
iPP-1.0	10.6	7.6	3.0	19.3

It has been well established that the average L from oriented crystallites is generally larger than that of the unoriented ones,[41] and L of β-crystal is also larger than that of α-crystal.[42] Thus, it is understandable that the increase of L in the β-iPP samples can be ascribed to the formation of oriented crystallites and high content of the β-crystal. At the same time, it should be noted that the increase in crystallinity is also consistent with the thickening of the crystal lamellae. Especially for iPP-1.0, compared with iPP-0.2, the decrease of long period and l_c may be ascribed to the fact that higher concentration of β-NA can induce higher nucleation density and then lead to the formation of smaller crystallites. This can be also confirmed by the decrease of crystallite size in β-iPP samples as shown in the following section.

In addition to l_c, lateral dimension of crystalline lamellae (D) was also determined. D reveals the effect of the nucleating agent on the epitaxial growth of crystalline lamellae or kebabs, which can be estimated using the Warren approximation:[42]

$$\left(D = \frac{\sqrt{8\pi}}{\omega}\right) \tag{11}$$

where ω is the width of the Gaussian function. The fitting data are representatively shown in Figure 7, and the results are listed in Table 3. As can be seen, the addition of β-NA allows D to increase, which is in agreement with L. This would be also attributed to the fact that the presence of β-NA lowers the free energy barrier and promotes the epitaxial growth of crystalline lamellae (or kebabs).[43]

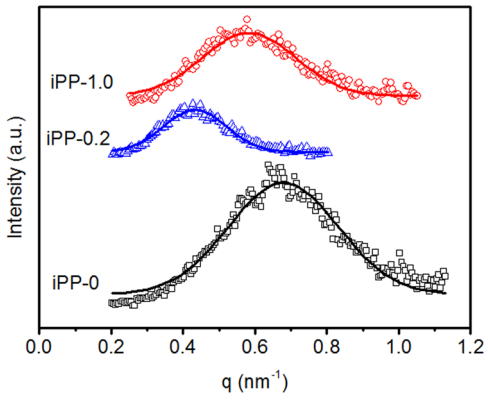

Figure 7. Plots of Iq^2 versus q. Solid lines are fitted data using the Gaussian method.

Crystallite Parameters. The crystallite size of each plane can be calculated from diffraction peaks of WAXD using the Scherrer equation:[44]

$$L_{hkl} = \frac{K\lambda}{\beta_{hkl}\cos\theta_{hkl}} \tag{12}$$

where L_{hkl} is the crystallite diameter (hkl), λ is the wavelength of the X-ray, K is crystallite shape factor, θ_{hkl} is the Bragg angle, and β_{hkl} is the full width of the diffraction line at half-maximum intensity measured in radians. Table 4 shows the crystallite size

Table 4. Crystallite Size and d-Spacing for Different β-NA Contents in iPP Samples

	d-spacing (Å)			L_{hkl} (nm)		
sample	110	040	300	110	040	300
iPP-0	6.246	5.210		13.3	14.1	
iPP-0.2	6.249	5.224	5.485	13.0	19.9	26.5
iPP-1.0	6.246	5.217	5.485	13.0	16.7	23.7

L_{hkl} and the d-spacing of crystal planes. Generally, the crystallite size L_{hkl} and d-spacing of crystal planes for iPP-0, iPP-0.2, and iPP-1.0 are apt to elevate first and then decrease with the increasing concentration of β-NA. Note that the tendency of crystallite size L_{hkl} and d-spacing of crystal planes are consistent with the variation of the long period and lamellar thickness. The results confirm our above conclusion that the decrease of a long period is attributed to the fact that a higher concentration of β-NA induces a much higher nucleation density. Moreover, the decreases of crystallite size L_{300} in β (300) for iPP-0.2 and iPP-1.0 should be attributed to the changes of orientation in the β-crystal.

As well-known, shear flow preferentially enhances the growth rate of crystallites and a higher nucleation density.[19,30,43] In addition, the addition of additives such as nucleating agents can also dramatically alter the crystallization kinetics and the final morphology. As demonstrated, the combined effects of shear and the addition of additives has been proven to produce a synergistic increase in the number of active nuclei and accelerating crystallization rates further than their individual contribution.[45−47] In our case, with the increase of β-NA content, the value of critical shear rate decreases and the nucleation density increases. With the help of shear flow, β-NA is oriented parallel to flow direction (see Figure S4 in Supporting Information) and promotes the formation of shish in the vicinity of β-NA. Because of the high content of β-NA in iPP-1.0, after the shear flow, more shishes are formed,[48,49] and meanwhile, there are more primary nuclei on the shish. Since there are more primary nuclei and shishes in a confined space, the growth of lamellae tends to be inhibited, resulting in a smaller size.[34,50] Therefore, compared to that in iPP-0.2, a smaller long period and smaller l_c, D, and L_{hkl} are obtained in iPP-1.0. Accordingly, a schematic is proposed to explain the effect of β-NA content on the flow-induced shish-kebab formation, which is shown in Figure 8.

CONCLUSION

The effect of β-NA on the crystalline structure in the oriented shear zone of injection molded iPP was investigated using 2D-WAXD and -SAXS. Lamellar branching of the α-crystal was

dx.doi.org/10.1021/ie401162c | Ind. Eng. Chem. Res. 2013, 52, 11996−12002

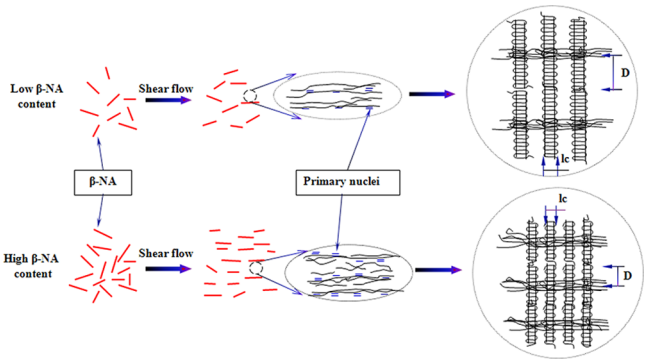

Figure 8. Schematic illustration of the effect of β-NA content on the flow induced shish-kebab formation.

found in iPP regardless of the β-NA concentration. Meanwhile, the fraction of daughter lamellae increases with the increasing content of β-NA. Interestingly, analogous to the lamellar branching of the α-crystal, similar parent−daughter lamellar branching of a novel crystalline morphology of the β-crystal was found only in iPP containing a higher content of β-NA (iPP-1.0). In addition, the long period, crystal lamellar thickness, and lateral dimension, d-spacing and crystallite size are found to be increased and then decrease with the increasing β-NA. The results demonstrate that the concentrations of β-NA have a significant effect on the crystal grain structure.

■ ASSOCIATED CONTENT

Ⓢ Supporting Information

Additional figures as described in the text. This material is available free of charge via the Internet at http://pubs.acs.org.

■ AUTHOR INFORMATION

Corresponding Author

*E-mail: gqzheng@zzu.edu.cn, ctliu@zzu.edu.cn.

Present Address

[§](X.L.) University of Erlangen through the support of the state scholarship fund of China Scholarship Council.

Notes

The authors declare no competing financial interest.

■ ACKNOWLEDGMENTS

The authors express thanks to the National Science Foundation of China (51173171, 11172271, 11172272) and HASTIT of Henan Province, State Key Laboratory of Materials Processing and Die & Mold Technology as well as The Key Laboratory of Polymer Processing Engineering, Ministry of Education, China. We also thank Prof. Liangbin Li from NSRL in USTC for his constructive discussion.

■ REFERENCES

(1) Meille, S. V; Bruckner, S.; Porzio, W. γ-Isotactic Polypropylene: A Structure with Nonparallel Chain Axes. *Macromolecules* **1990**, *23*, 4114−4121.

(2) Lotz, B.; Graff, S.; Straupe, C.; Wittmann, J. C. Single Crystals of γ Phase Isotactic Polypropylene: Combined Diffraction and Morphological Support for a Structure with Non-parallel Chains. *Polymer* **1991**, *32*, 2902−2910.

(3) Varga, J. β-Modification of Isotactic Polypropylene: Preparation, Structure, Processing, Properties, and Application. *J. Macromol. Sci. B.* **2002**, *41*, 1121−1171.

(4) Varga, J.; Karger-Kocsis, J. Interfacial Morphologies in Carbon Fibre-Reinforced Polypropylene Microcomposites. *Polymer* **1995**, *36*, 4877−4884.

(5) Dragaun, H.; Hubeny, H.; Muschik, H. Shear-Induced β-form Crystallization in Isotactic Polypropylene. *J. Polym. Sci. Polym. Phys.* **1977**, *15*, 1779−1799.

(6) Byelov, D.; Panine, P.; Remerie, K.; Biemond, E.; Alfonso, G. C; de Jeu, W. H. Crystallization under Shear in Isotactic Polypropylene Containing Nucleators. *Polymer* **2008**, *49*, 3076−83.

(7) Koscher, E.; Fulchiron, R. Influence of Shear on Polypropylene Crystallization: Morphology Development and Kinetics. *Polymer* **2002**, *43*, 6931−6942.

(8) Grigoryeva, O. P; Karger-Kocsis, J. Melt Grafting of Maleic Anhydride onto an Ethylene−Propylene−Diene Terpolymer (EPDM). *Eur. Polym. J.* **2000**, *36*, 1419−1429.

(9) Huy, T. A; Adhikari, R.; Lupke, T.; Henning, S.; Michler, G. H. Molecular Deformation Mechanisms of Isotactic Polypropylene in α- and β-Crystal Forms by FTIR Spectroscopy. *J. Polym. Sci. Polym. Phys.* **2004**, *42*, 4478−4488.

(10) Xiao, W. C; Wu, P. Y; Feng, J. C; Yao, R. Y. Effect of Beta-Nucleating Agents on Crystallization and Melting Behavior of Isotactic Polypropylene. *J. Appl. Polym. Sci.* **2008**, *108*, 3370−3379.

(11) Zhang, N.; Zhang, Q.; Wang, K.; Deng, H.; Fu, Q. Combined Effect of Beta-nucleating Agent and Multi-walled Carbon Nanotubes on Polymorphic Composition and Morphology of Isotactic Polypropylene. *J. Therm. Anal. Calorim.* **2012**, *107*, 733−743.

(12) Stocker, W.; Schumacher, M.; Graff, S.; Thierry, A.; Wittmann, J. C; Lotz, B. Epitaxial Crystallization and AFM Investigation of a Frustrated Polymer Structure: Isotactic Poly(propylene), β Phase. *Macromolecules* **1998**, *31*, 807−814.

(13) Zhou, J. J; Liu, J. G; Yan, S. K; Dong, J. Y; Li, L.; Chan, C. M; Schultz, J. M. Atomic Force Microscopy Study of the Lamellar Growth of Isotactic Polypropylene. *Polymer* **2005**, *46*, 4077−4087.

(14) Zipper, P.; Janosi, A.; Geymayer, W.; Ingolic, E.; Fleischmann, E. Comparative X-ray Scattering, Microscopical, and Mechanical Studies on Rectangular Plates Injection Molded from Different Types of Isotactic Polypropylene. *Polym. Eng. Sci.* **1996**, *36*, 467−482.

(15) Housmans, J. W; Gahleitner, M.; Peters, G. W. M; Meijer, H. E. H. Structure−Property Relations in Molded, Nucleated Isotactic Polypropylene. *Polymer* **2009**, *50*, 2304−2319.

(16) Fujiyama, M.; Wakino, T.; Kawasaki, Y. Structure of Skin Layer in Injection-Molded Polypropylene. *J. Appl. Polym. Sci.* **1988**, *35*, 29−49.

(17) Zhong, G. J; Li, Z. M; Li, L. B; Mendes, E. Crystalline Morphology of Isotactic Polypropylene (iPP) in Injection Molded Poly(ethylene terephthalate) (PET)/iPP Microfibrillar Blends. *Polymer* **2007**, *48*, 1729−1740.

(18) Sun, T. C; Chen, F. H; Dong, X.; Zhou, Y.; Wang, D. J; Han, C. C. Shear-Induced Orientation in the Crystallization of an Isotactic Polypropylene Nanocomposite. *Polymer* **2009**, *50*, 2465−2471.

(19) Kumaraswamy, G.; Verma, R. K; Kornfield, J. A; Yeh, F.; Hsiao, B. S. Shear-Enhanced Crystallization in Isotactic Polypropylene. In-Situ Synchrotron SAXS and WAXD. *Macromolecules* **2004**, *37*, 9005−9017.

(20) Matsuba, G.; Sakamoto, S.; Ogino, Y.; Nishida, K.; Kanaya, T. Crystallization of Polyethylene Blends under Shear Flow. Effects of Crystallization Temperature and Ultrahigh Molecular Weight Component. *Macromolecules* **2007**, *40*, 7270−7275.

(21) Liu, X. H; Zheng, G. Q; Dai, K.; Jia, Z. H; Li, S. W; Liu, C. T; Chen, J. B; Shen, C. Y; Li, Q. Morphological Comparison of Isotactic Polypropylene Molded by Water-Assisted Injection Molding and Conventional Injection Molding. *J. Mater. Sci.* **2011**, *46*, 7830−7838.

(22) Zhu, P. W; Edward, G. Morphological Distribution of Injection-moulded Isotactic Polypropylene: a Study of Synchrotron Small Angle X-ray Scattering. *Polymer* **2004**, *45*, 2603−2613.

(23) Picken, S. J; Aerts, J.; Visser, R.; Northolt, M. G. Structure and Rheology of Aramid Solutions: X-ray Scattering Measurements. *Macromolecules* **1990**, *23*, 3849−3854.

(24) Turner-Jones, A.; Aizlewood, J.; Beckett, D. Crystalline Forms of Isotactic Polypropylene. *Macromol. Chem. Phys.* **1964**, *75*, 134−154.
(25) Zhu, P. W; Edward, G. Orientational Distribution of Parent−Daughter Structure of Isotactic Polypropylene: A Study Using Simultaneous Synchrotron WAXS and SAXS. *J. Mater. Sci.* **2008**, *43*, 6459−6467.
(26) Zhu, P. W; Phillips, A.; Tung, J.; Edward, G. Orientation Distribution of Sheared Isotactic Polypropylene Plates through Thickness in the Presence of Sodium Benzoate. *J. Appl. Phys.* **2005**, *97*, 104908.
(27) Balzano, L. Flow induced crystallization of polyolefins. Ph.D. Thesis, Technische Universiteit Eindhoven, 2008.
(28) Luo, F.; Geng, C. Z; Wang, K.; Deng, H.; Chen, F.; Fu, Q.; Na, B. New Understanding in Tuning Toughness of β-Polypropylene: The Role of β-Nucleated Crystalline Morphology. *Macromolecules* **2009**, *42*, 9325.
(29) Somani, R. H; Yang, L.; Hsiao, B. S; Agarwal, P. K; Fruitwala, H. A; Tsou, A. H. Shear-Induced Precursor Structures in Isotactic Polypropylene Melt by in-Situ Rheo-SAXS and Rheo-WAXD Studies. *Macromolecules* **2002**, *35*, 9096−9104.
(30) Dukovski, I.; Muthukumar, M. Langevin Dynamics Simulations of Early Stage Shish-Kebab Crystallization of Polymers in Extensional Flow. *J. Chem. Phys.* **2003**, *118*, 6648−6655.
(31) Lotz, B.; Wittmann, J. C. The Molecular Origin of Lamellar Branching in the α (Monoclinic) Form of Isotactic Polypropylene. *J. Polym. Sci., Polym. Phys.* **1986**, *24*, 1541−1558.
(32) Wang, Y.; Pan, J. L; Mao, Y. M; Li, Z. M; Li, L. B; Hsiao, B. S. Spatial Distribution of γ-Crystals in Metallocene-Made Isotactic Polypropylene Crystallized under Combined Thermal and Flow Fields. *J. Phys. Chem. B* **2010**, *114*, 6806−6816.
(33) Lotz, B.; Wittmann, J. C.; Lovinger, A. J. Structure and Morphology of Poly(propylenes): A Molecular Analysis. *Polymer* **1996**, *37*, 4979−4992.
(34) Phillips, A. W; Zhu, P. W; Hadinata, C.; Edward, G. Crystallization and Melting of Oriented Parent−Daughter. Lamellae in Sheared Isotactic Poly(propylene). *Aust. J. Chem.* **2010**, *63*, 1179−1188.
(35) Yalcin, B.; Valladares, D.; Cakmak, M. Amplification Effect of Platelet Type Nanoparticles on the Orientation Behavior of Injection Molded Nylon 6 Composites. *Polymer* **2003**, *44*, 6913−6925.
(36) Xiao, W. C; Wu, P. Y; Feng, J. C. Influence of a Novel β-Nucleating Agent on the Structure, Morphology, and Nonisothermal Crystallization Behavior of Isotactic Polypropylene. *J. Appl. Polym. Sci.* **2009**, *111*, 1076−1085.
(37) Zhao, S. C.; Cai, Z.; Xin, Z. A highly Active Novel β-Nucleating Agent for Isotactic Polypropylene. *Polymer* **2008**, *49*, 2745−2754.
(38) Luo, F.; Wang, K.; Ning, N. Y; Geng, C. Z; Deng, H.; Chen, F.; Fu, Q.; Qian, Y. Y; Zheng, D. Dependence of Mechanical Properties on β-Form Content and Crystalline Morphology for β-Nucleated Isotactic Polypropylene. *Polym. Adv. Technol.* **2011**, *22*, 2044−2054.
(39) Strobl, G.; Schneider, M. Direct Evaluation of the Electron Density Correlation Function of Partially Crystalline Polymers. *J. Polym. Sci. Polym. Phys.* **1980**, *18*, 1343−1359.
(40) Liu, G. M; Zheng, L. C; Zhang, X. Q; Li, C. C; Jiang, S. C; Wang, D. J. Reversible Lamellar Thickening Induced by Crystal Transition in Poly(butylene succinate). *Macromolecules* **2012**, *45*, 5487−5493.
(41) Chen, Y. H; Mao, Y. M; Li, Z. M; Hsiao, B. S. Competitive Growth of α- and β-Crystals in β-Nucleated Isotactic Polypropylene under Shear Flow. *Macromolecules* **2010**, *43*, 6760−6771.
(42) Larin, B.; Avila-Orta, C. A; Somani, R. H; Hsiao, B. S; Marom, G. Combined Effect of Shear and Fibrous Fillers on Orientation-Induced Crystallization in Discontinuous Aramid Fiber/Isotactic Polypropylene Composites. *Polymer* **2008**, *49*, 295−302.
(43) Zhu, P. W; Edward, G.; Nichols, L. Effect of Additives on Distributions of Lamellar Structures in Sheared Polymer: A Study of Synchrotron Small-Angle X-ray Scattering. *J. Phys. D. Appl. Phys.* **2009**, *42*, 245406.
(44) Alexander, L. E. *X-ray Diffraction Methods in Polymer Science*; Wiley: New York, 1976.
(45) Rozanski, A.; Monasse, B.; Szkudlarek, E.; Pawlak, A.; Piorkowska, E.; Galeski, A.; Haudin, J. M. Shear-Induced Crystallization of Isotactic Polypropylene Based Nanocomposites with Montmorillonite. *Eur. Polym. J.* **2009**, *45*, 88−101.
(46) Huo, H.; Jiang, S. C; An, L. J; Feng, J. C. Influence of Shear on Crystallization Behavior of the β Phase in Isotactic Polypropylene with β-Nucleating Agent. *Macromolecules* **2004**, *37*, 2478−2483.
(47) Phillips, A. W; Bhatia, A.; Zhu, P. W; Edward, G. Shish Formation and Relaxation in Sheared Isotactic Polypropylene Containing Nucleating Particles. *Macromolecules* **2011**, *44*, 3517−3528.
(48) Zheng, G. Q; Jia, Z. H; Liu, X. H; Liu, B. C; Zhang, X. L; Dai, K.; Shao, C. G; Zheng, X. J; Liu, C. T; Cao, W.; et al. Enhanced Orientation of the Water-Assisted Injection-Molded iPP in the Presence of Nucleating Agent. *Polym. Eng. Sci.* **2012**, *52*, 725−732.
(49) Schrauwen, B. A. G; Breemen, L. C. A. V; Spoelstra, A. B; Govaert, L. E; Peters, G. W. M; Meijer, H. E. H. Structure, Deformation, and Failure of Flow-Oriented Semicrystalline Polymers. *Macromolecules* **2004**, *37*, 8618−8633.
(50) Cao, J.; Lü, Q. F. Crystalline Structure, Morphology and Mechanical Properties of β-Nucleated Controlled-Rheology Polypropylene Random Copolymers. *Polym. Test.* **2011**, *30*, 899−906.